perature. This increased thermal motion results in an increase in the molar volume and can affect the twist of the helical axis by either (i) increasing the average displacement angle of one molecule with respect to its neighbor or (ii) increasing the intermolecular distance along the helical axis. Process i will result in an increased twist with increase in temperature, while, under comparable conditions, process ii will decrease the twist of the mesophase.

A similar proposal can be made for lyotropic mesophases where the nematogenic unit is the micelle rather than the molecule. It has been pointed out, however, that in micellar systems process i can occur both at the molecular level and at the micellar level.[17] The evidence discussed above suggests that the conformational distribution of the headgroup is not much affected by the temperature range of this study, certainly not in comparison to the effects of variation in concentration. In addition, the overall headgroup alignment is also insensitive to temperature (Tables IV and V). This suggests that process i, described above, is inactive at the level of the chiral amphiphiles. The decrease in twist with increase in temperature can then be ascribed to a dominating effect of process ii.

On the basis of the above arguments, the result of a change in temperature is a change in the average intermicelle distance along the helical axis. With cooling, this average distance decreases and the resultant twist is larger. Other effects of changes in temperature such as the changes in the motional properties of the amphiphiles within the micelles probably are much less important, at least for the temperature range of this study. This conclusion is drawn because the headgroup alignment, as defined by the dipolar couplings and the N–D deuterium quadrupole splittings, is almost a constant between 292 and 310 K (Table V).

Acknowledgment. Thanks are gratefully extended to the Natural Sciences and Engineering Research Council of Canada for its support of this work.

Registry No. L-KDDA-α-d_2, 139914-26-4; L-DDA-α-d_2, 139914-25-3; L-KDDA-d_{23}, 139914-27-5; KCl, 7447-40-7; dodecyl aldehyde, 112-54-9; 2,2-dideuteriododecyl aldehyde, 129355-47-1; 2,2-dideuteriododecanioic acid, 64118-39-4; 2,2-dideuteriododecanoyl chloride, 139914-24-2; sodium L-alaninate, 16480-55-0; decanol, 112-30-1; D,L-alanine, 302-72-7; L-alanine, 56-41-7.

---

(17) Tracey, A. S.; Radley, K. *Langmuir* **1990**, *6*, 1221–1224.

Intermediate Liquid Crystalline Phases in the Binary System $C_{16}TACl–H_2O$: An NMR and Low-Angle X-ray Diffraction Study

Ulf Henriksson,*

Department of Physical Chemistry, Royal Institute of Technology, S-100 44 Stockholm, Sweden

Eunice S. Blackmore, Gordon J. T. Tiddy,

Unilever Research, Port Sunligt Laboratory, Quarry Road East, Bebington, Wirral,
Merseyside L63 3JW England

and Olle Söderman

Division of Physical Chemistry 1, University of Lund, P.O. Box 124, S-221 00 Lund, Sweden
(Received: September 13, 1991)

The liquid crystalline phases formed in the concentration range between the hexagonal and the lamellar phase in the binary system $C_{16}TACl–H_2O$ have been studied by ^2H, ^{14}N, and ^{35}Cl NMR, low-angle X-ray diffraction and optical microscopy. A cubic phase and three anisotropic so-called intermediate phases have been found. At 45 °C the hexagonal phase is stable up to 75 wt % $C_{16}TACl$. Between 75% and 79%, a biaxial phase (Int-1) built up by long rods with noncircular cross sections is formed. From the asymmetry parameter of the time-averaged electric field gradient tensor the axial ratio of the cross section was found to increase from ~1.15 to ~1.4 with increasing concentration. In the range 80–83% a second intermediate phase (Int-2) is formed with a smaller quadrupole splitting than in the hexagonal phase and with an asymmetry parameter close to 1. A third intermediate phase (Int-3) was detected in some samples. This uniaxial phase has a very small quadrupole splitting (4.4 kHz for ^2H in the α-methylene segment). It is suggested that the Int-2 and Int-3 phases are built up by noncubic periodic minimal surfaces, e.g., tetragonally, rhombohedrally, or orthorhombically distorted P or D surfaces.

Introduction

A major problem currently attracting the attention of researchers on lyotropic liquid crystals is to understand the complex array of structures tha can form in the transition region between the lamellar phase (L_α) and normal and reversed hexagonal phases (H_1 and H_2 respectively).[1-11] Monoalkyl surfactants usually form H_1 rather than H_2 phases;[12-14] hence with these materials the problem concerns surfactant aggregates having a curvature that is concave toward the nonpolar micellar core. This provides a limitation on the smallest dimension of any micelles formed due to the alkyl chain packing constraint,[15] which might simplify the

---

(1) Charvolin, J.; Sadoc, J. F. *J. Phys. Chem.* **1988**, *92*, 5787.
(2) Rancon, Y.; Charvolin, J. *J. Phys. Chem.* **1988**, *92*, 2646.
(3) Rancon, Y.; Charvolin, J. *J. Phys. Chem.* **1988**, *92*, 6339.
(4) Andersson, S.; Hyde, S. T.; Larsson, K.; Lidin, S. *Chem. Rev.* **1988**, *88*, 221.
(5) Hyde, S. T. *J. Phys. Chem.* **1989**, *93*, 1458.
(6) Siegel, D. P. *Biophys. J.* **1986**, *49*, 1155.
(7) Siegel, D. P. *Biopys. J.* **1986**, *49*, 1171.
(8) Lindblom, G.; Brentel, I.; Sjölund, M.; Wikander, G.; Wieslander, A. *Biochemistry* **1986**, *25*, 7502.
(9) Rilfors, L.; Eriksson, P.-O.; Arivdsson, G.; Lindblom, G. *Biochemistry* **1986**, *25*, 7702.
(10) Kirk, G. L.; Gruner, S. M.; Stein, D. L. *Biochemistry* **1984**, *23*, 1093.
(11) Anderson, D.; Gruner, S. M.; Leibler, S. *Proc. Natl. Acad. Sci. U.S.A.* **1988**, *85*, 5364.
(12) Luzatti, V. In *Biological Membranes*; Chapman, D., Ed.; Academic Press: London, 1968; Vol. 1, p 71.
(13) Winsor, P. A. *Chem. Rev.* **1968**, *68*, 1.
(14) Ekwall, P. *Adv. Liq. Cryst.* **1971**, *1*, 1.
(15) Israelachvili, J. N.; Mitchell, D. J.; Ninham, B. W. *J. Chem. Soc., Faraday Trans. 1* **1976**, *72*, 1525.

0022-3654/92/2096-3894$03.00/0

problem. (The packing constraint simply states that the minimum micelle dimension cannot exceed the length of two all-trans alkyl chains.)[15] In previous reports we have investigated the mesophases formed in this composition region for sodium and potassium soaps,[16] sodium alkyl sulfates,[16,17] a range of cationic surfactants,[18] polyoxyethylene nonionic surfactants,[19,20] and zwitterionic surfactants.[21] A general pattern of behavior is observed for all these materials. For short alkyl chains the phase sequence is (for the structure of "intermediate" phases see below)

hexagonal (H_1) → biocontinuous cubic (V_1) → lamellar (L_α)

For long alkyl chains the phase sequence changes to

hexagonal (H_1) → "intermediate" (Int) → lamellar (L_α)

Obviously, for some medium "transition" chain lengths the sequence $H_1 \rightarrow Int \rightarrow V_1 \rightarrow L_\alpha$ can occur. The length of the paraffin chain for this transition in behavior appears to increase with head group size. We have suggested that a balance between alkyl chain flexibility and head group curvature determines whether V_1 or Int phases occur, with flexibility favoring V_1.[20] Fluorocarbon surfactants, where the chains are much stiffer than hydrocarbon chains, form V_1 phases less readily for ionic surfactants, in agreement with this.[20] A large range of structures appear to be possible for the intermediate phases,[12,16,17,22,23] ranging from elliptical rod phases (related to H_1), through 2-D arrays of short rods (lamellar phase with holes, related to L_α), to (possibly) 3-D noncubic, regular networks (related to V_1; see below). The most detailed study to date is the elegant work of Kékicheff and Cabane[22] on sodium dodecyl sulfate, where the advantages of a synchrotron X-ray source were employed to identify an elliptical rod phase (related to H_1), an orthorhombic or rhombohedral structure, a tetragonal structure (possibly related to L_α), and a V_1 phase. In our earlier work on cationic surfactants[18] we demonstrated that, for alkyl trimethylammonium chlorides (C_nTACl), the phase sequence is $H_1/V_1/L_\alpha$ for $n < 12$, while for $n = 16$ and 18, the sequence $H_1/Int/L_\alpha$ changes to $H_1/V_1/L_\alpha$ on heating. For some temperatures the sequence $H_1/Int/V_1/Int/L_\alpha$ is observed. In a previous paper[24] we presented some of our results obtained by polarizing microscopy, differential scanning calorimetry (dsc), multinuclear magnetic resonance spectroscopy (NMR), and X-ray diffraction. First, the known H_1 and L_α phases of $C_{12}TACl$ were examined to provide a model system for the behavior of the NMR spectra. The hexagonal, lamellar, and gel regions of $C_{16}TACl$ were delineated, and a partial phase diagram was described. Hexadecyltrimethylammonium chloride ($C_{16}TACl$) was selected as a good candidate for a detailed study because the structures of the intermediate phases and the nature of the Int → V_1 transition could be investigated. In this system it was also possible to prepare monophasic samples of the intermediate phases large enough to be used for NMR spectroscopy, and in this work, we report ^2H, ^{14}N, and ^{35}Cl spectra from three anisotropic intermediate phases in this system along with some optical microscopy and X-ray data. NMR spectra from quadrupolar nuclei can give valuable information about the aggregate geometry in lyotropic liquid crystals since the rapid self-diffusion of the surfactant molecules over the aggregate causes a partial averaging of the quadrupole interaction and the magnitude and symmetry of the remaining time-averaged quadrupole interaction, which can be determined from the NMR spectrum, are sensitive to the aggregate shape and curvature. We were not successful in fully identifying the mesophase structures, although we were able to detect at least two very different Int types and to determine that the Int/V_1 phase transitions are first order. Considerable problems were caused by some metastability of the Int phases, so that heating and cooling sequences give different results.

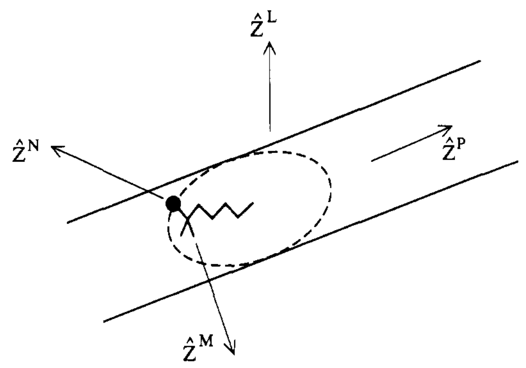

Figure 1. Schematic picture of a biaxial surfactant aggregate and definitions of the different directions used in the theoretical description of the ^2H NMR spectrum from such an aggregate. $\hat{z}^L$ is the direction of the external magnetic field B_0.

Experimental Section

Materials. $C_{16}TACl$ (Eastman Kodak) was recrystallized from acetone, vacuum-dried, and stored in a desiccator. The $C_{16}TACl$-α-d_2 was prepared by reacting hexadecanoyl chloride (Fluka, 98%) with dimethylamine to produce the corresponding *N,N*-dimethylamide which was reduced with $LiAlD_4$. The resulting hexadecyldimethylamine-α-d_2 was then quaternized with methyl chloride. The purity of the labeled $C_{16}TACl$ was checked with ^1H NMR. It was also found that the labeled and unlabeled material gave the same phase transitions (vide infra), which further confirms the purity. Heavy water (BDH, ≥99.7%) and ^2H-depleted water (Stohler Isotope Chemicals) were used as supplied. The samples for the NMR measurements were prepared by weighing into glass ampules with ~7-mm inner diameter which were flame sealed. The size of the samples was ≤200 mg, and they were homogenized by centrifugation and kept at 39 °C for several days before the measurements. The phase behavior of the samples were reproducible over several years, which shows that no decomposition of the surfactant occurred. All compositions given in this paper (except in Figure 3) have been corrected for differences in isotope composition and refer to the natural isotope composition.

Methods. The optical microscopy, the low-angle X-ray diffraction, and the ^{14}N and ^{35}Cl NMR measurements as well as the ^2H measurements on ^2H_2O were performed as described in previous work.[24] For the ^2H-labeled surfactant the ^2H NMR spectra were recorded at 30.7 MHz on a Bruker MSL-200 spectrometer using a 10-mm multinuclear high-resolution saddle coil probe. The quadrupole echo method[25] was used, the length of a 90° pulse was 10 μs, and the distance between the 90 °C pulses was 25 μs. The digitization rate was 1 μs, and the start of the data accuisition was carefully adjusted to the maximum of the quadrupole echo. The repetition rate was 4–10 s^{-1}. The sample temperature was controlled with a Bruker VT-1000 temperature regulator. The air flow was kept as high as possible in order to minimize temperature gradients.[26] The temperature was measured repeatedly using a platinum resistance thermometer and it was found to be constant within ±1 °C.

NMR Spectra from Liquid Crystalline Phases

Both ^2H and ^{14}N have spin $I = 1$ and moderately high electric quadrupole moments, consequently their NMR spectra from liquid

---

(16) Rendall, K.; Tiddy, G. J. T.; Trevethan, M. A. *J. Chem. Soc., Faraday Trans. 1* **1983**, *79*, 637.

(17) Leigh, I. D.; McDonald, M. P.; Wood, R. M.; Tiddy, G. J. T.; Trevethan, M. A. *J. Chem. Soc., Faraday Trans. 1* **1982**, *77*, 2867.

(18) Blackmore, E. S.; Tiddy, G. J. T. *J. Chem. Soc., Faraday Trans. 1* **1988**, *84*, 1115.

(19) Mitchell, D. J.; Tiddy, G. J. T.; Waring, L.; Bostock, T.; McDonald, M. P. *J. Chem. Soc., Faraday Trans. 1* **1983**, *79*, 975.

(20) Hall, C.; Tiddy, G. J. T. In *Surfactants in Solution*; Mittal, K. L., Ed.; Plenum Press: New York, 1989; Vol. 1, p 9.

(21) Tiddy, G. J. T., unpublished results.

(22) Kékicheff, P.; Cabane, B. *J. Phys.* **1987**, *48*, 1571.

(23) Kékicheff, P.; Tiddy, G. J. T. *J. Phys. Chem.* **1989**, *93*, 2520.

(24) Blackmore, E. S.; Tiddy, G. J. T. *Liq. Cryst.* **1990**, *8*, 131.

(25) Davis, J.H.; Jeffrey, K. R.; Bloom, M.; Valic, M. I.; Higgs, T. P. *Chem. Phys. Lett.* **1976**, *42*, 390.

(26) Allerhand, A.; Addleman, R. E.; Osman, D. *J. Am. Chem. Soc.* **1985**, *107*, 5809.

crystals are governed by the time-independent quadrupole Hamiltonian[27]

$$\hat{H}_Q{}^{\circ} = \langle \hat{H}_Q(t) \rangle = \frac{1}{4}\frac{eQ\langle V_{zz}\rangle^L}{h}[3\hat{I}_z^2 - 2] \qquad (1)$$

which gives two absorption lines centered around the Larmor frequency

$$\nu_{\pm} = \nu_0 \pm \frac{3}{4}\frac{eQ\langle V_{zz}\rangle^L}{h} \qquad (2)$$

where eQ is the nuclear electric quadrupole moment and $\mathbf{V}$ is the electric field gradient (efg) tensor at the nucleus. The superscript L denotes a laboratory-fixed coordinate system defined by the external magnetic field B_0 (Figure 1) and $\langle V_{zz}\rangle^L$ is the component of the time-averaged efg tensor along B_0.

For covalently bound nuclei the efg is usually of intramolecular origin, i.e., the components of the efg tensor are constant in a frame fixed in the surfactant molecule. For ^{2}H in a methylene segment, the efg tensor is to a good approximation cylindrically symmetric and its molecule fixed principal axis system (M) is directed along the carbon–deuterium bond.[28] In this paper we will use the following values for the quadrupole coupling constant (χ) and the asymmetry parameter of the efg tensor (η):[28]

$$\chi(^2\mathrm{H}) = eQV_{zz}^M/h = 181 \text{ kHz} \qquad (3)$$

$$\eta^M(^2\mathrm{H}) = (V_{xx}^M - V_{yy}^M)/V_{zz}^M \approx 0 \qquad (4)$$

It is more difficult to determine the components of the ^{14}N efg tensor in alkyltrimethylammonium ions,[29–31] and they may vary slightly with aggregate shape.

Due to the molecular motions, the components of the efg tensor in the L frame are time dependent, and according to eq 2, it is the time-average $\langle V_{zz}\rangle^L$ that determines the NMR spectrum. In surfactant aggregates molecular motions occur on different time scales. Fast local motions like trans–gauche isomerizations, and torsional oscillations usually have effective correlation times $\tau_c^f \sim 10^{-11}$–10^{-10} s. On a time scale longer than τ_c^f, molecular motions over distances of the same magnitude as the aggregate size occur due to lateral diffusion of the surfactant molecules over the aggregate surface and in some systems reorientation of the whole aggregates can also take place. We denote the motionally averaged principal components of the efg tensor on this longer time scale $\langle V_{zz}\rangle^P$, $\langle V_{yy}\rangle^P$, and $\langle V_{xx}\rangle^P$. Since according to the Poisson equation the efg tensor is traceless, it is sufficient to use two independent quantities and usually the largest principal component of the time-averaged efg tensor $\langle V_{zz}\rangle^P$ and the aggregate asymmetry parameter

$$\eta^P = (\langle V_{xx}\rangle^P - \langle V_{yy}\rangle^P)/\langle V_{zz}\rangle^P \qquad (5)$$

are used. Note that η^P can be $\neq 0$ even if $\eta^M = 0$. $\langle V_{zz}\rangle^L$, which according to (2) determines the observed quadrupole splitting, can be expressed in $\langle V_{zz}\rangle^P$ and η^P through the coordinate transformation

$$\langle V_{zz}\rangle^L = \langle V_{zz}\rangle^P\left[D_{00}^{(2)}(\Omega_{LP}) + \frac{\eta^P}{\sqrt{6}}(D_{02}^{(2)}(\Omega_{LP}) + D_{0-2}^{(2)}(\Omega_{LP}))\right] =$$
$$\langle V_{zz}\rangle^P\left[\frac{1}{2}(3\cos^2\Theta_{LP} - 1) + \frac{\eta^P}{2}(\sin^2\Theta_{LP}\cos 2\varphi_{LP})\right] \qquad (6)$$

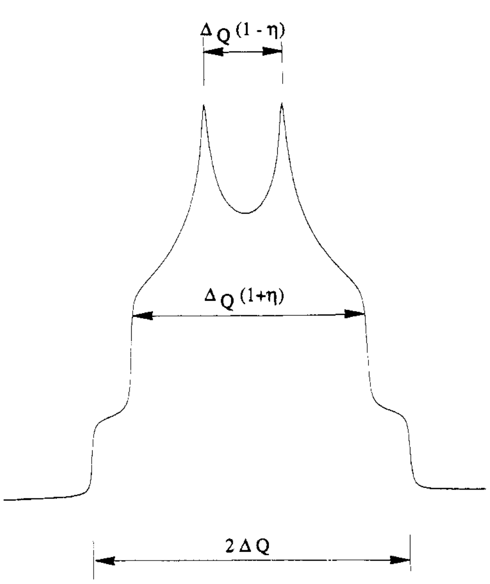

Figure 2. Simulated NMR line shape for a powder sample with $I = 1$ and an asymmetric efg tensor ($\eta = 0.5$). The Lorentzian line broadening used corresponds to 2% of the quadrupole splitting.

where the polar angle Θ_{LP} and the azimuthal angle φ_{LP} define the orientation of the principal axis system of the motionally averaged efg tensor relative to the laboratory system and $D_{pq}^{(2)}(\Omega)$ are elements of the second-order Wigner rotation matrix.

As seen from eqs 2 and 6, the NMR spectrum for a given fixed aggregate orientation Ω_{LP} is determined by the averages $\langle V_{zz}\rangle^P$ and η^P. For a sample where all orientations are equally probable, a so-called powder spectrum is obtained. Figure 2 shows a simulation of the line shape[32] of such a spectrum. The important quantities $\langle V_{zz}\rangle^P$ and η^P can be determined directly from the frequency difference between the two outer edges and from the difference between the two inner peaks. If the quadrupole splitting Δ_Q is defined as half the distance between the outer edges in the spectrum we have

$$\Delta_Q = \frac{3}{4}\frac{eQ\langle V_{zz}\rangle^P}{h} \qquad (7)$$

In systems containing surfactant aggregates, the fast local motions (effective correlation time τ_c^f) and the slower motions over distances of the magnitude of the aggregate size are uncorrelated and they usually occur on well-separated time scales. This means that the averaging of the efg tensor can be treated as a two-step process.[33]

$$V^M \xrightarrow{\text{local motions}} \langle V\rangle^N \xrightarrow{\text{aggregate motions}} \langle V\rangle^P \qquad (8)$$

The time-averaged efg tensor $\langle V\rangle^N$ on a time scale somewhat longer than τ_c^f is axially symmetric, with its principal axis parallel to a local normal to the aggregate surface provided that there is at least threefold symmetry around the normal. This condition is not strictly fulfilled for a cylindrical aggregate, but it is expected to be a good approximation for nuclei located near the surfactant head group.[34] $\langle V\rangle^N$ is then given by

$$\langle V_{zz}\rangle^N = V_{zz}^M S^{\mathrm{loc}} \qquad (9)$$

where S^{loc} is a local order parameter with respect to a local surface normal.

$$S^{\mathrm{loc}} = \langle D_{00}^{(2)}(\Omega_{MN})\rangle_{\mathrm{f}} + \frac{\eta^M}{\sqrt{6}}\langle D_{02}^{(2)}(\Omega_{MN}) + D_{0-2}^{(2)}(\Omega_{MN})\rangle_{\mathrm{f}} =$$
$$\frac{1}{2}\langle 3\cos^2\Theta_{MN} - 1\rangle_{\mathrm{f}} + \frac{\eta^M}{2}\langle\sin^2\Theta_{MN}\cos 2\varphi_{MN}\rangle_{\mathrm{f}} \qquad (10)$$

---

(27) Abragam, A. *Principles of Nuclear Magnetism*; Oxford University Press: Oxford, 1961; Chapter VII.

(28) Söderman, O.; Henriksson, U. *J. Chem. Soc., Faraday Trans. 1* **1987**, *83*, 1515.

(29) Henriksson, U.; Ödberg, L.; Eriksson, J. C.; Westman, L. *J. Phys. Chem.* **1977**, *81*, 76.

(30) Pratum, T. K.; Klein, M. P. *J. Magn. Reson.* **1983**, *53*, 473.

(31) Söderman, O.; Walderhaug, H.; Henriksson, U.; Stilbs, P. *J. Phys. Chem.* **1985**, *89*, 3693.

(32) Bloembergen, N.; Rowland, T. J. *Acta Metall.* **1953**, *1*, 731.

(33) Halle, B.; Wennerström, H. *J. Chem. Phys.* **1981**, *75*, 1928.

(34) Quist, P.-O.; Halle, B. *Mol. Phys.* **1988**, *65*, 547.

The subscript f indicates averaging due to the fast local motion. The slower aggregate motions cause a further averaging of the efg tensor, and on a time scale longer than $1/\Delta_Q$ we have[34]

$$\langle V_{zz}\rangle^P = V_{zz}^M \frac{1}{2}\langle S^{\mathrm{loc}}(3\cos^2\Theta_{PN} - 1)\rangle_{\mathrm{agg}} \tag{11}$$

$$\eta^P = 3\,\frac{\langle S^{\mathrm{loc}}\sin^2\Theta_{PN}\cos 2\varphi_{PN}\rangle_{\mathrm{agg}}}{\langle S^{\mathrm{loc}}(3\cos^2\Theta_{PN} - 1)\rangle_{\mathrm{agg}}} \tag{12}$$

The local order parameter S^{loc} is different for different methylene segments in the alkyl chain. In addition, for a certain methylene segment it may be a function of the position on the aggregate due to, for example, different curvature and packing conditions at different positions on the aggregate. However, there is experimental evidence from many binary surfactant systems[28,35] that such variations are rather small and we can as a reasonable approximation treat S^{loc} as a constant, i.e.

$$\langle V_{zz}\rangle^P = V_{zz}^M S^{\mathrm{loc}} \frac{1}{2}\langle 3\cos^2\Theta_{PN} - 1\rangle_{\mathrm{agg}} \tag{13}$$

$$\eta^P = 3\,\frac{\langle \sin^2\Theta_{PN}\cos 2\varphi_{PN}\rangle_{\mathrm{agg}}}{\langle 3\cos^2\Theta_{PN} - 1\rangle_{\mathrm{agg}}} \tag{14}$$

When the averaging in the second step in (8) is due to lateral diffusion over the aggregate, the resulting averages $\langle V_{zz}\rangle^P$ and η^P can give direct information about the aggregate shape and symmetry. For a lamellar phase with planar bilayers $\Theta_{PN} = 0°$, and for a hexagonal phase with circular cylinders $\Theta_{PN} = 90°$, which give the expected results

$$\langle V_{zz}\rangle^P_{\mathrm{lam}} = V_{zz}^M S^{\mathrm{loc}} \tag{15}$$

$$\langle V_{zz}\rangle^P_{\mathrm{hex}} = -\frac{1}{2} V_{zz}^M S^{\mathrm{loc}} \tag{16}$$

$$\eta^P_{\mathrm{lam}} = 0 \tag{17}$$

$$\eta^P_{\mathrm{hex}} = 0 \tag{18}$$

The so-called *ribbon phase* has been studied by Chidichimo et al.[36,37] This biaxial phase is built up by rods with noncircular cross section, and the asymmetry parameter η^P can be used to deduce information about the axial ratio of the cross section of the rods (vide infra).

For aggregate structures with cubic symmetry and for micellar aggregates, the time average of the efg tensor in the L frame vanishes and the NMR spectrum is a single line at the Larmor frequency.

The equations above hold for ^2H and ^{14}N, which both have spin $I = 1$. For ^{35}Cl the same considerations apply for the $\pm^3/_2 \rightarrow \pm^1/_2$ transitions.[27]

Results

Phase Behavior. The phase diagram for $C_{16}TACl$ based on microscopy, NMR, and X-ray diffraction is shown in Figure 3. All the phase boundaries shown correspond to those occurring on slow heating. The H_1, V_1, L_α, and gel phases have been described in the previous report.[24] In this work we report NMR and other measurements from three anisotropic Int phases in the region between the hexagonal and the lamellar phases.

Optically, the Int-1 phase, which is stable between 75% and 79% at 45 °C, is almost indistinguishable from the H_1 phase as are its bulk viscosity and appearance. The texture observed is the "nongeometric" type of Rosevear[38] (Figure 4a) with a somewhat decreased birefringence from H_1, and more defined "lines". However, these latter features are subjective and certainly could not be employed to identify the structure. The Int-2 region (80–83% at 45 °C) gives the distinctive texture shown in Figure 4b. This texture does somewhat resemble that obtained with other Int phases such as those of lithium perfluorooctanoate or hexaoxyethylene glycol hexadecyl ether,[20] but the resemblance is not

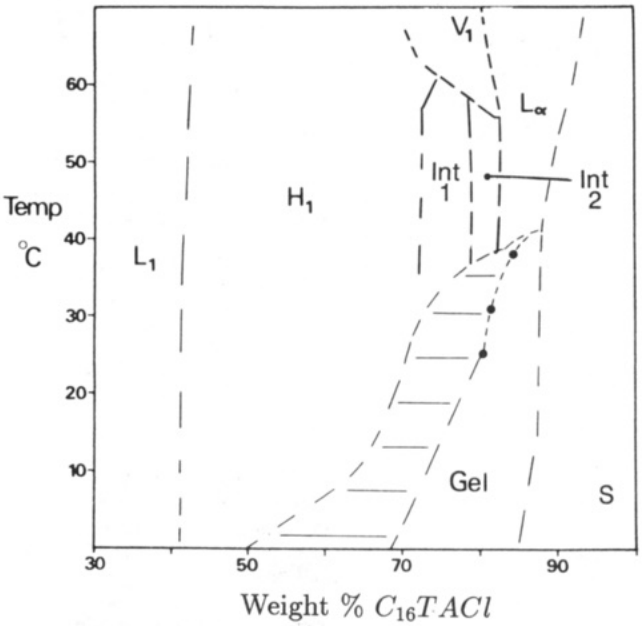

Figure 3. Partial phase diagram for the binary system $^2H_2O-C_{16}TACl$. The phases shown are those that occur on slow heating of samples: L_1, micellar solution; H_1, hexagonal phase; L_α, lamellar phase; Gel, monolayer interdigited gel phase; V_1, biocontinuous cubic phase; Int-1 and Int-2, intermediate phases—see text for details. Note that the compositions refer to $^2H_2O-C_{16}TACl$ mixtures while all other compositions given in this paper refer to the natural isotope composition.

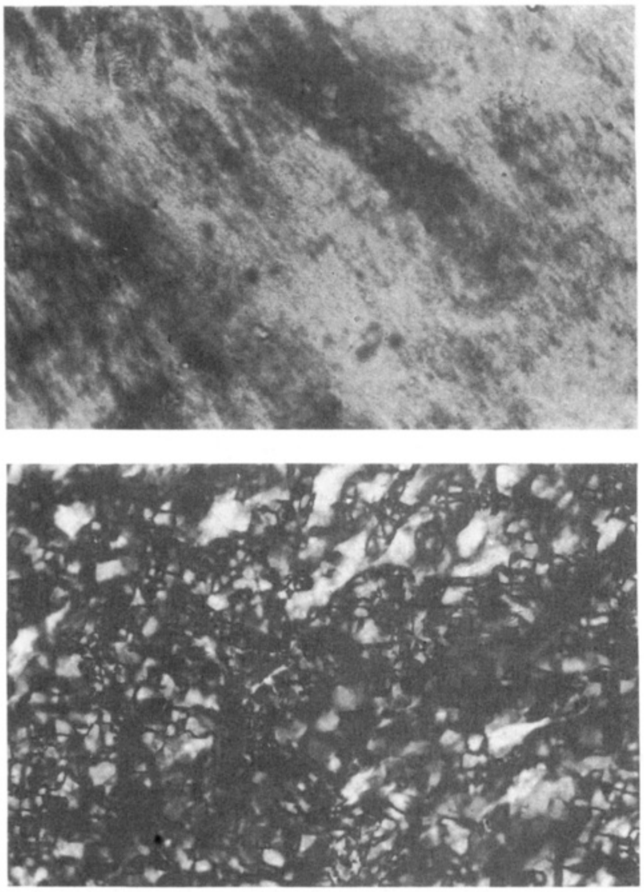

Figure 4. Optical microscope textures for the phases Int-1 (a, top) and Int-2 (b, bottom) (crossed polars, 45 °C, ca. ×200; photographs reduced 55% for publication).

---

(35) Mély, B.; Charvolin, J.; Keller, P. *Chem. Phys. Lipids* **1975**, *15*, 161.

(36) Chidichimo, G.; Vaz, N. A. P.; Yaniv, Z.; Doane, J. W. *Phys. Rev. Lett.* **1982**, *49*, 1950.

(37) Chidichimo, G.; Golemme, A.; Doane, J. W.; Westerman, P. W. *J. Chem. Phys.* **1985**, *82*, 536.

(38) Rosevear, F. B. *J. Am. Oil Chem. Soc.* **1954**, *31*, 628.

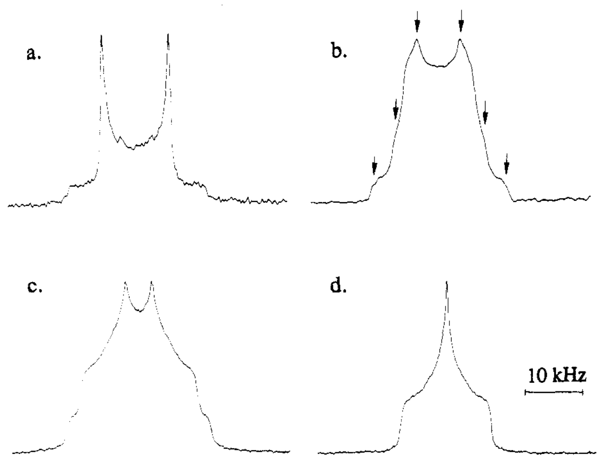

Figure 5. Experimental ^2H spectra at 45 °C for α-deuterated $C_{16}TACl$ in aqueous samples with 70.2% (a), 75.1% (b), 77.7% (c), and 81.3% (d) surfactant (the compositions refer to the natural isotope composition). (b) is a spectrum from a two-phase sample H_1/Int-1, with the arrows indicating absorptions due to the Int-1 phase.

sufficiently close for structure identification to be made.

Note that cooling samples in the V_1 region did not result in reversible transitions to the Int-1 or Int-2 phases. Frequently the V_1 phase, once formed, was stable for days. Even on cooling to the gel region (where a large exothermic transition occurs), the V_1 phase was stable for hours. Given the length of time required to establish equilibrium behavior, we have limited this study to the phase structures formed on slow heating.

^2H NMR of α-^2H Labeled $C_{16}TACl$. Figure 5 shows some typical ^2H NMR spectra from α-deuterated $C_{16}TACl$ at 45 °C in the composition range 70–85% surfactant. The spectra from the hexagonal phase H_1 in the range 70–74% are powder spectra for a cylindrically symmetric efg tensor ($\eta^P = 0$) with a practically constant quadrupole splitting $\Delta_Q = 12.0$ kHz, which, using $\chi = 181$ kHz for the quadrupole coupling constant, gives an order parameter $|S^{loc}| = 0.177$ in good agreement with previous measurements at 27 °C and at 60 °C.[31,39]

The spectra from the Int-1 phase show that it is biaxial with an asymmetry parameter η^P increasing from 0.53 to 0.69. The quadrupole splitting is very close to that of the H_1 phase, which supports the notion that this phase is built up by long parallel rods. At 75.1% a two-phase spectrum from the biaxial Int-1 phase and the uniaxial H_1 phase was recorded (Figure 5b).

The Int-2 phase gives ^2H spectra with a quadrupole splitting considerably smaller than in the H_1 phase and with a nonzero asymmetry parameter η^P which rapidly increases to 1 with increasing concentration. For concentrations above ~81%, this phase transforms to the cubic V_1 phase after ~24 h at 45 °C while it is stable for longer time at the lower concentrations.

For concentrations above 83%, the uniaxial lamellar phase L_α with a quadrupole splitting about tiwce the splitting in the hexagonal phase is observed. The quadrupole splittings and the asymmetry parameters as functions of the $C_{16}TACl$ concentration in the different phases are presented in Figure 6.

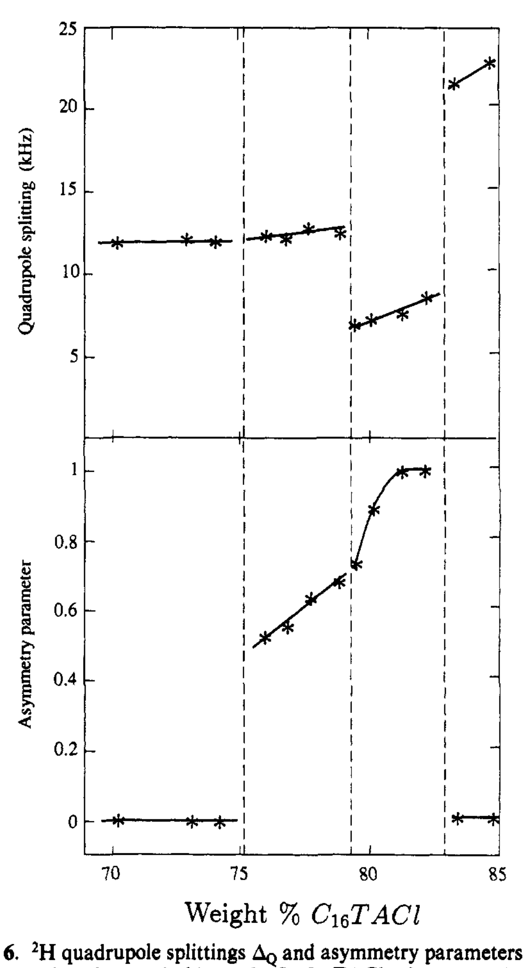

Figure 6. ^2H quadrupole splittings Δ_Q and asymmetry parameters η^P for α-deuterated surfactant in binary H_2O–$C_{16}TACl$ mixtures at 45 °C as functions of the composition. The compositions refer to the natural isotope composition.

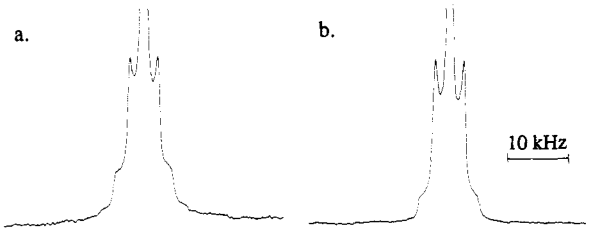

Figure 7. ^2H spectra from the Int-3 phase containing α-deuterated $C_{16}TACl$: (a) 76.5% $C_{16}TACl$, 60 °C; (b) 78.9% $C_{16}TACl$, 45 °C. In these samples, a 1:9 D_2O–H_2O mixture was used as solvent and the central line is from the HDO. The compositions refer to the natural isotope composition.

Some samples containing α-deuterated surfactant were prepared with a 1:9 mixture D_2O–H_2O in order to rapidly monitor the phase transformations. For two of these samples a third intermediate phase (Int-3) was observed in the ^2H NMR spectra (Figure 7). This uniaxial phase has a very small quadrupole splitting for the α-methylene segment, about one-third of that in the hexagonal phase. Despite hard efforts, it was not possible to observe the Int-3 phase for samples prepared with the ^2H-depleted water. Whether the existence of this phase depends on the isotope composition of the solvent, on different chemical purity of the water, or on the storage history of the samples cannot be settled at present. The observed ^2H quadrupole splitting from the Int-3 phase is 4.4 kHz. This is much higher than the D_2O splitting observed in the L_α phase[24] and the powder patterns in Figure 7 can thus safely be assigned to originate from the labeled surfactant molecules.

Other NMR Data for $C_{16}TACl$–^2H_2O Mixtures. As in the previous study,[24] ^2H, ^{14}N, and ^{35}Cl measurements were made on unlabeled surfactant–^2H_2O mixtures. The ^{14}N and ^{35}Cl spectra were recorded with an old NMR spectrometer, and they were of much lower quality than the ^2H spectra in Figure 5 (for typical spectra, see ref 24). It was, however, possible to determine the ^{14}N quadrupole coupling constants with reasonable accuracy. The ^{14}N spectra showed that the region 75–79% surfactant (weights adjusted to the normal water scale) consisted of the Int-1 phase while Int-2 occurred over 80–83%, in good agreement with the results from samples containing labeled surfactant and H_2O. As is shown in Figure 8, the Δ_Q and η^P values for ^{14}N are remarkably similar to those for ^2H, giving even more confidence in both sets of data. The ^2H spectra from ^2H_2O were much less informative in this region. Samples from the Int-1 phase gave a broad singlet with line widths of a few hundred hertz and no discernable structure. Presumably this arises from rapid water diffusion

---

(39) Sjöberg, M.; Henriksson, U.; Wärnheim, T. *Langmuir* **1990**, *6*, 1205.

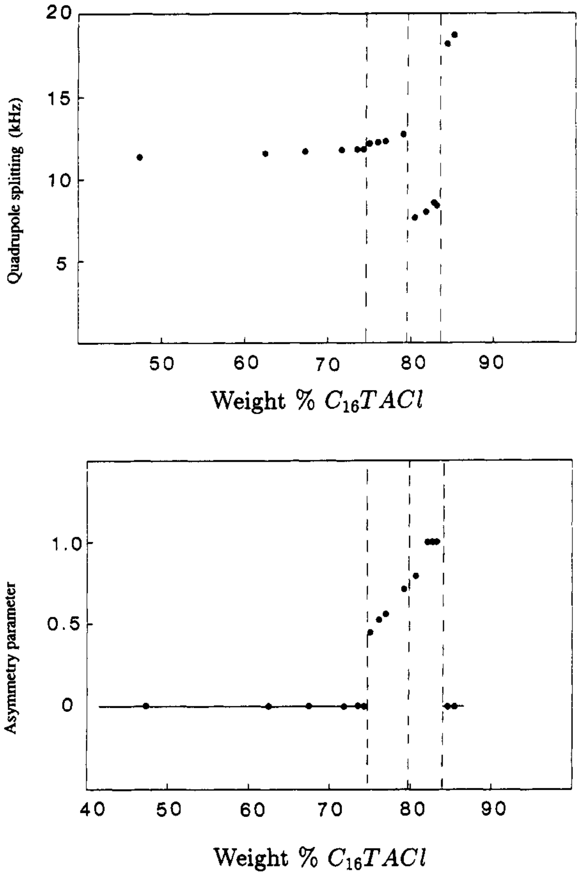

Figure 8. ^{14}N quadrupole splittings Δ_Q and asymmetry parameters η^P for binary $^2H_2O-C_{16}TACl$ mixtures at 45 °C as functions of the composition. The compositions refer to the natural isotope composition.

between crystallites having different macroscopic orientations which partially averages the spectra. The Int-2 samples gave apparently uniaxial powder patterns with $\Delta_Q(^2H) = 115 - 145$ Hz. This compares with $\Delta_Q(^2H) \approx 250$ and 1000 Hz at the highest H_1 and lowest L_α concentrations, respectively.[24] Clearly this result differs significantly from the surfactant spectra described above (Figures 6 and 8).

For the ^{35}Cl resonance uniaxial spectra were obtained from the H_1 and L_α phases,[24] but only one Int-1 sample gave a recognizable biaxial spectrum (77.4% $C_{16}TACl$, 45 °C, $\Delta_Q(^{35}Cl) = 15$ kHz, $\eta^P = 0.48$). This single biaxial result is entirely consistent with the α-$^2H_2$ and ^{14}N data. All the remaining Int-phase samples gave broad featureless spectra (except for the sharp central line). The rapid diffusion of Cl^- ions between different crystallites can explain the absence of structural features in the spectra, and the observation that different samples show different degrees of averaging in their spectra can be seen as an indication that the crystallite size differs from sample to sample.

Further ^{14}N measurements on unlabeled surfactant samples were made as a function of temperature to investigate the nature of phase transitions between intermediate and other phases. In particular it was of interest to observe if the asymmetry parameter approached zero at the boundary with a uniaxial phase. Figures 6 and 8 indicate that this does not occur at the H_1/Int-1 or Int-2/L_α boundaries. The data reported in Table I confirm this observation. Thus, these phase transitions are always first order in the present system.

X-ray Diffraction. The results from small-angle X-ray diffraction experiments performed at 45 °C and covering a range from 52% to 82% $C_{16}TACl$ are presented in Figure 9. Only one diffraction line is obtained up to 74% $C_{16}TACl$. Starting at 75%, one additional line appears. The Bragg spacing of this additional line increases with increasing $C_{16}TACl$ concentration up to ~80% $C_{16}TACl$. At $C_{16}TACl$ concentrations above 80% its *d* value decreases. Also included in Figure 9 are the phase boundaries as obtained from the NMR data presented above (Figure 6).

TABLE I: ^{14}N **NMR Data for Various** $C_{16}TACl-^2H_2O$ **Samples as a Function of Temperature**

wt % $C_{16}TACl^a$	temp, °C	Δ_Q, kHz	η^P	phases present
75.0	45	12.1	0.44	Int-1
	50	11.9	0.40	Int-1
	55	11.9	0.38	Int-1 +
		11.9	0	+ H_1
	57	11.7	0	H_1
	60	11.3	0	H_1 +
		0	0	+ V_1 (trace)
76.1	45	12.3	0.56	Int-1
	55	11.8	0.55	Int-1
	57	11.7	0.51	Int-1
	60	11.7	0.4	Int-1 +
		0	0	+ V_1
81.9	44	13.0	0.72	Int-1
	46	13.3	0.77	Int-1
	48	two phases		Int-1 + Int-2
	50	7.9	1.0	Int-2
82.7	39	8.4	1.0	Int-2
	42	8.8	0.92	Int-2
	46	17.1	0	L_α

[a] The compositions refer to the natural isotope composition.

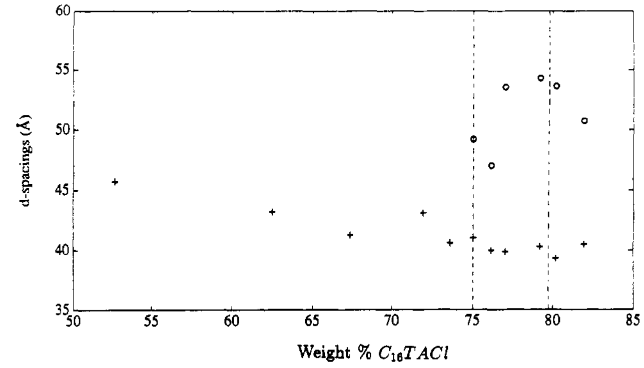

Figure 9. Bragg spacings at 45 °C from liquid crystalline phases in the $C_{16}TACl-H_2O$ system. The vertical lines indicate the phase boundaries, obtained from the NMR work.

Evidently, the NMR and X-ray data are in excellent agreement as regards the phase behavior at 45 °C. Thus the diffraction line below 75% is obtained from the hexagonal phase, while the two lines between 75% and 80%, with *d* values above and below the hexagonal *d* value close to the phase boundary, correspond to the Int-1 phase. Above 80% the data probably correspond to the Int-2 phase. However, because of the influence of sample history observed by NMR for the Int-1/Int-2 transition (vide infra) and the difference in sample size between the two techniques we cannot be completely certain which phase is present at the highest concentration. We were unable to obtain good X-ray data at the highest levels of surfactant.

Metastable-Phase Formation. Most of the behavior reported above is entirely reproducible provided that samples are not left for weeks in the gel + H_1 two-phase region and that the same temperature treatment is employed. For example, the unlabeled surfactant-^2H_2O samples heated from ambient temperature to 45 °C gave mainly reproducible behavior over ~4 years (1982–1987). The data shown in Figure 8 represent the average of up to six measurements separated in time by 3–4 years. The reproducibility of $\Delta_Q(^{14}N)$ is ±0.3 kHz while $\eta^P(^{14}N)$ is reproducible to better than ±0.04. However, for a sample containing 81.9% $C_{16}TACl$, gradual heating gave Int-1 (see Table I) while immediate heating to 45 °C gave Int-2. This behavior was observed from both ^2H_2O and ^{14}N resonances. From ^2H_2O resonance, the uniaxial pattern of the Int-2 phase ($\Delta_Q = 115$ Hz) took ca. 40 min to develop from Int-1 at 40 °C following the complete disappearance of the gel phase. Above and below this concentration the samples attained the equilibrium-phase structure (Int-1 or L_α) within ca. 5–10 min, usually less than 3 min. Note that *T*-jump experiments have established that even where viscous V_1

phases are involved in phase transitions, raising the temperature 1 °C above the phase transition is enough to cause the change in less than 10 s.[40] Also, the fact that η^P and Δ_Q for the 81.9% Int-1 sample at 44 and 46 °C are larger than the values in Figure 8 shows that this behavior is genuine metastability rather than slow mixing of the samples. The observation of the Int-3 phase with some samples and not others (see above) may also arise from this type of mesophase metastability.

Discussion

Intermediate liquid crystalline phases in the binary system SDS–H_2O have recently been studied in some detail by Kékicheff et al.,[22,41,42] using samples with a water concentration gradient and spatially resolved X-ray diffraction with synchrotron radiation among other techniques. Four phases were identified in the composition range between the hexagonal and the lamellar phase: (i) a two-dimensional *monoclinic* phase, (ii) a three-dimensional *rhombohedral* or *orthorhombic* phase, (iii) a three-dimensional *cubic* phase, and (iv) a three-dimensional *tetragonal* phase.

The two-dimensional monoclinic phase can be seen as a deformed hexagonal phase built up by rods with noncircular cross sections and with a unit cell which is a parallelogram that can be considered as a gradual deformation of the rhomb of the hexagonal unit cell, so that the obtuse angle is reduced from 120° and the lengths of the four sides are no longer equal. This phase is identical with the so-called ribbon phase studied by Chidichimo et al.[37] The phase denoted Int-1 in the $C_{16}TACl–H_2O$ system can be identified with this two-dimensional monoclinic phase. This phase is biaxial since it has two unique directions, the axis of the parallel rods and the long axis of the noncircular cross section. The observed asymmetry parameter η^P in this phase is clearly related to the axial ratio of the cross sections of the rods. Chidichimo et al.[37] considered a *ribbon model* with a cross section consisting of a central rectangular part with a semicircle on each side, while Quist and Halle[34] have presented a detailed analysis of NMR spectra from rods with elliptical cross sections. The quantitative difference between these two approaches is not very large,[34] and we will use this *elliptical model* to analyze our data. When the rods are continuously deformed, there is a gradual transition to a lamellar bilayer structure. However, for small deformations, the largest component of the efg tensor remains along the axis of the rods and the quadrupole splitting therefore stays constant while the asymmetry parameter increases (Figure 10). For a certain deformation, the components of the efg tensor along the rod and along the long axis of the cross section become equal. In this case $\eta^P = 1$, and for further deformations, the asymmetry parameter decreases and the quadrupole splitting increases toward their values in the lamellar phase. Since the observed quadrupole splitting in the Int-1 phase in the $C_{16}TACl$ system has the same value as in the hexagonal phase and the asymmetry parameter increases with the concentration, the former so-called small-deformation regime applies.

The observed asymmetry parameter depends mainly on the axial ratio of the noncircular cross section of the aggregates, but it is also affected by nonuniform orientational order and/or surface density.[34] The assumption of a uniform (i.e., curvature-independent) orientational order for the α-methylene segment, which has been used in eqs 13 and 14, is probably a good approximation since the local order parameter is practically the same in the hexagonal as in the lamellar phase (see Figure 6). Furthermore, order parameters determined from the analysis of frequency-dependent relaxation in spherical micelles of cationic and anionic surfactants[43-45] are close to the local order parameters measured in the corresponding hexagonal phases. Figure 10a shows the calculated quadrupole splitting as a function of the axial ratio of the elliptical cross section of the rods, assuming uniform orientational order and surface density. In the small-deformation

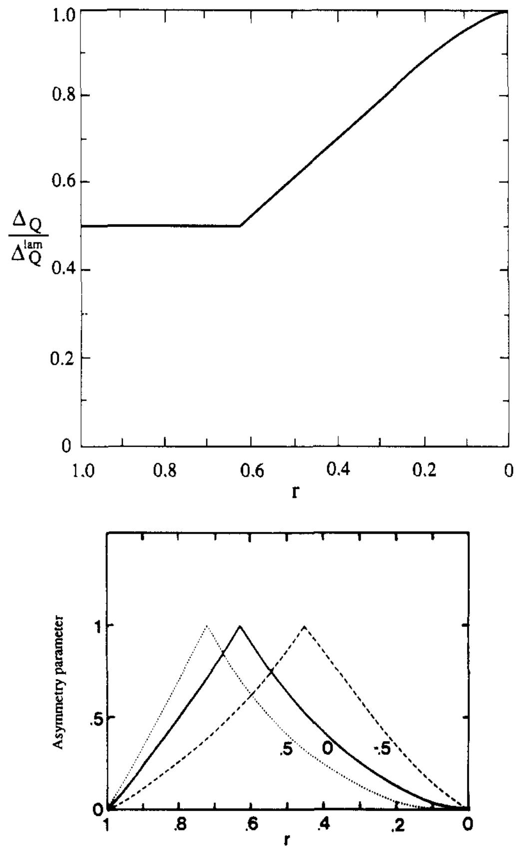

Figure 10. (a, top) Calculated quadrupole splittings for a cylindrical rod with elliptical cross section as functions of the ratio r = short axis/long axis, assuming uniform orientational order and surface distribution. (b, bottom) Calculated asymmetry parameters for a cylindrical rod with elliptical cross section as functions of the ratio r = short axis/long axis. The parameter values shown in the figure characterize the deviation from uniform orientational order and surface distribution where zero corresponds to the uniform case. For a uniform orientational order, a positive value for this parameter corresponds to a preference for the surfactant molecules of residing in the low-curvature parts of the aggregates. From ref 34, where details about the calculations can be found.

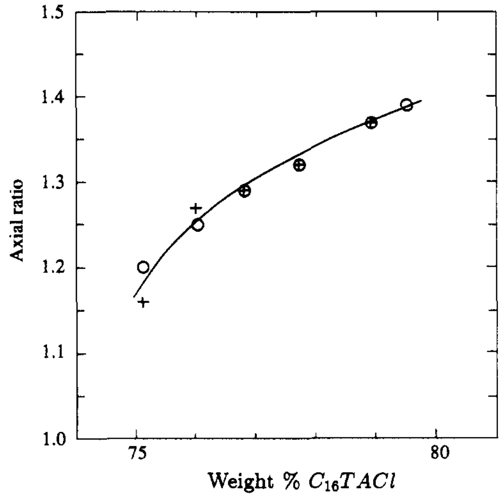

Figure 11. Axial ratio for the cross sections of the rods in the Int-1 phase evaluated from the experimental asymmetry parameters using the elliptical rod model with uniform orientational order and surface distribution:[34] O, 313 K; +, 318 K.

---

(40) Knight, P.; Wyn-Jones, E.; Tiddy, G. J. T. *J. Phys. Chem.* **1985**, *89*, 3447.

(41) Kékicheff, P.; Gabrielle-Madelmont, C.; Ollivon, M. *J. Colloid Interface Sci.* **1989**, *131*, 112.

(42) Kékicheff, P. *J. Colloid Interface Sci.* **1989**, *131*, 133.

(43) Söderman, O.; Carlström, G.; Olsson, U.; Wong, T. C. *J. Chem. Soc., Faraday Trans. 1* **1988**, *84*, 4475.

(44) Söderman, O.; Henriksson, U.; Olsson, U. *J. Phys. Chem.* **1987**, *91*, 116.

(45) Ginley, M.; Henriksson, U.; Li, P. *J. Phys. Chem.* **1990**, *94*, 4644.

TABLE II: Geometrical Parameters at 45 °C Determined from the X-ray Diffraction Data in Figure 9

wt % $C_{16}TACl$	phase	r_{hc}, Å	β, deg
52.6	H_1	18.2	120
62.5	H_1	18.6	120
67.4	H_1	18.4	120
71.9	H_1	19.8	120
73.6	H_1	18.9	120
75.0	Int-1		114
76.1	Int-1		126
77.0	Int-1		117
79.2	Int-1		116

regime and with uniform orientational order, the splitting is independent of the surface distribution[34] while the asymmetry parameter depends on the surface density distribution on the aggregates (Figure 10b). Figure 11 shows the axial ratios for the cross section of the rods in the Int-1 phase calculated from the experimental asymmetry parameters using the elliptical model and the assumption of uniform orientational order and surface density. A nonuniform surface distribution with a preference for the surfactant molecules to reside in regions with low curvature will give somewhat smaller axial ratios than those presented in Figure 11, but the difference is quite small as can be seen from Figure 10b.

The spectrum in Figure 5b and the data in Table I show that there is a two-phase region between the H_1 and Int-1 phases. In molten mesophases containing ionic surfactants, it is unlikely that there is any large composition heterogeneity unless the samples have been stored close to a phase boundary with a large composition difference. This is not the case here (see Experimental Section), and these phases can be considered as difference phases in the sense of the phase rule. In the Int-1 phase, which is in equilibrium with the hexagonal phase, the axial ratio of the noncircular cross section is ~1.15. With increasing surfactant concentration, the axial ratio increases to ~1.4 at the highest concentration at which the phase is stable.

In order to obtain information about the dimensions of the surfactant aggregates from the X-ray diffraction data in Figure 9, we need the densities of the different parts of the liquid crystal. In accordance with previous work, we will use 0.89 g/cm^3 for the density of $C_{16}TACl$ and 462.2 Å^3 for the volume of a hexadecyl chain.[46-49] In addition, we assign the C_{16} alkyl chain to the hydrophobic core of the aggregates, while the trimethylammonium chloride part of the surfactant plus the water makes up the hydrophilic region of the liquid crystal. This choice is dictated by the fact that the trimethylammonium head group is hydrated, while the number of water molecules penetrating into the hydrocarbon core is certainly very small. The value for the radius of the hydrocarbon core, r_{hc}, for the hexagonal phase can be obtained from the relation[12]

$$r_{hc} = [2d^2\phi/\pi\sqrt{3}]^{1/2} \qquad (19)$$

where d is the value of the first-order Bragg spacing and ϕ is the volume fraction of the hydrocarbon core. Calculated r_{ch} values for the hexagonal phase are presented in Table II. Close the phase boundary to the monoclinic phase, $r_{hc} \approx 19$ Å. The all-trans length of a C_{16} chain is 21.7 Å.[49] Thus, the value of r_{hc} corresponds roughly to 90% of the length of the all-trans chain.

For the two-dimensional monoclinic lattice, the unit cell is a parallelogram with the obtuse angle, β, given by[50]

$$\cos(\beta - 90) = \phi d_{10}d_{01}/\pi ab \qquad (20)$$

Here d_{hk} is the Bragg spacing of a diffraction line with Miller indices h and k (we restrict ourselves to the diffraction line corresponding to $hk = 10$ and $hk = 01$), while a and b are the major and minor semiaxes of the cross section of the surfactant rods. We have chosen to compute the angle β from eq 20. In order to do so, we assume that the minor semiaxis is equal to the value of r_{hc} in the hexagonal phase close to the phase boundary. Moreover, we have used axial ratios a/b from Figure 11, which were evaluated from the NMR data using the elliptical model as described above. In this way we obtain the values for β that are presented in Table II. There is some scatter in the calculated β values, but they center around 116° and do not vary much over the rather narrow concentration region of the monoclinic phase. The value of β is close to the value obtained for the same phase in the binary SDS–water system at 55 °C,k where $\beta = 114.1°$ was found.[22]

The two phases Int-2 and Int-3 both have quadrupole splittings that are considerably smaller than those of the hexagonal phase. One possible cause for a small quadrupole splitting can be the existence of small ordered nonspherical aggregates as in the lyotropic nematic phases.[51] However, considering the high surfactant concentration and the high viscosity of the intermediate phases in the $C_{16}TACl-H_2O$ system, this must be considered as a very unlikely structure in the present case (the viscosity of the Int-2 phase is slightly smaller than in the cubic V_1 phase). It is more reasonable to assume that these phases contain three-dimensional networks but with lower symmetry than the bicontinuous cubic phase V_1. In fact, the rhombohedral or orthorhombic phase and the tetragonal phase observed by Kêkicheff et al. in the $SDS-H_2O$ system[22,41,42] can be seen as originating from bicontinuous cubic V_1 phases which have been deformed in one or two directions. The averaging of the efg tensor due to lateral diffusion of surfactant molecules over the bicontinuous aggregate structure is thus not complete as in the cubic phases.

Due to the limited number of relfections in the X-ray diffraction results it is usually not possible to make an unambiguous assignment of the structure of the bicontinuous cubic phases. The aggregate structure in these phases is often assumed to be related to so-called infinite periodic minimal surface (IPMS), which have zero mean curvature in all points. Several such surfaces with cubic and with lower symmetry have been described.[4,52-54] Recently, Anderson[55] has calculated the quadrupole splittings for molecules that are free to diffuse on tetragonally or rhombohedrally distorted P or D surfaces. Such distortions give rise to NMR spectra with nonzero quadrupole splittings and asymmetry parameters $\eta^P = 0$, and they can thus serve as models for the structure of the Int-3 phase. The P and D surfaces as well as their distorted analogues (P_t, D_t and P_r, D_r, respectively) are adjoint surfaces,[52] which implies that they will give the same NMR spectrum.[55] The P and D structures can be continuously contracted to any arbitrary degree of distortion while they can only be stretched to a critical degree of distortion.[52]

The experimental value for the quadrupole splitting in the Int-3 phase is $\Delta_Q(3) = 0.182\Delta_Q(L_\alpha)$. The calculations of Anderson[55] show that this value can be obtained by both tetragonal and rhombohedral distortions of the cubic D and P surfaces. For these two types of structure the deviation from cubic symmetry is determined by the value of a single parameter E, the so-called elevation parameter, in the Weierstrass polynomial which defines the equation of the minimal surface.[52] For the surface with tetragonal symmetry (P_t or D_t), the observed splitting in the Int-3 phase gives $E = 0.37$.[55] This value corresponds to a contraction of the cubic structure for which $E = 1/3^{1/2} \approx 0.577$.[52] Rhombohedrally distorted surfaces generally give rise to smaller quadrupole splittings, and for such a structure, the observed splitting in the Int-3 phase corresponds to a degree of distortion very close to the critical limit for the existence of the rhombohedrally distorted surface.[52,55]

---

(46) Reiss-Husson, F.; Luzatti, V. *J. Phys. Chem.* **1964**, *68*, 3504.

(47) Cabane, B. In *Surfactants in Solutions, New Methods of Investigation*; Zana, R., Ed.; Dekker: New York, 1987; p 57.

(48) Hayter, J. B.; Penfold, J. *Colloid Polym. Sci.* **1983**, *261*, 1022.

(49) Tanford, C. *The Hydrophobic Effect: Formation of Micelles and Biological Membranes*; Wiley: New York, 1973.

(50) *International Tables for Crystallography*; Hahn, T., Ed., D. Reidel: Dordrecht, The Netherlands, 1983; Vol. A.

(51) Hendrikx, Y.; Charvolin, J. *J. Phys.* **1981**, *42*, 1427.

(52) Lidin, S. *J. Phys.* **1988**, *49*, 421.

(53) Koch, E.; Fisher, W. *Z. Kristallogr.* **1988**, *183*, 129.

(54) Hyde, S. T. *Prog. Colloid Polym. Sci.* **1990**, *82*, 236.

(55) Anderson, D. M. *Colloq. Phys.* **1990**, *C7*, 1.

Orthorhombically distorted surfaces will give asymmetry parameters $\eta^P \neq 0$, and it is thus reasonable to tentatively assign such a structure to the Int-2 phase. Orthorhombic distortions are, however, considerably more difficult to treat mathematically since the integrals that have to be evaluated cannot be reduced to elliptic form. Work on this problem is under way and will be published separately. A real challenge is to account for the occurrence of a uniaxial ^{2}H spectrum from ^2H_2O and a biaxial spectrum from the labeled surfactant in the Int-2 phase.

As regards the X-ray diffraction lines for concentrations above 80% C_{16}TACl, we have not made any attempts to index these, since independent information about the phase structure is rather limited, and the numbers of diffraction lines are too few to make a structure determination based solely on the X-ray data meaningful. In conclusion, we feel that the main result of the X-ray investigation is the corroboration of the phase boundaries determined from the NMR experiments. In addition, some information about the surfactant aggregates comprising the liquid crystals is obtained. The observed quadrupole splittings and asymmetry parameters for the Int-2 and Int-3 phases cannot alone be used to determine the structures of these phases. However, they contain valuable information, since any proposed detailed geometry for the aggregates must be in agreement with them.

Finally, we consider the phenomenon of metastable-phase formation. Short-chain trimethylammonium cationic surfactants give V_1 cubic phases at compositions between H_1 and L_α rather than the intermediate phases.[18,20] The increase in stability of Int structures as alkyl chain length increases implies that some of these are likely to have very similar stabilities for some particular chain length derivatives, causing metastable phases to occur. The specific phases that are metastable will differ for different homologues and head groups. This is a problem that should occur widely for many long-chain surfactants ($n \geq 16$), but to date there are few reports of the phenomenon. One reason for this is that techniques to unambiguously assign structures have not been readily available. The increasing use of synchrotron X-ray equipment and high-frequency multinuclear NMR spectrometers should enable significant progress to be made in understanding the molecular mechanisms involved in these phase transformations, as well as providing many hours of frustration for research students.

Registry No. C_{16}TACl, 112-02-7.

Electron Spin Resonance Study of Lateral Diffusion of Ni^{2+} on Sodium Dodecyl Sulfate Micellar Surfaces

Masayuki Aizawa

Government Industrial Development Laboratory, Hokkaido, 2-17-2-1 Tsukisamu-Higashi, Toyohira-ku, Sapporo 062, Japan *(Received: October 25, 1991)*

Surface diffusion constants of Ni^{2+} on a sodium dodecyl sulfate (SDS) micelle are estimated through an analysis of spin exchange reaction of a hydrophobic nitroxide radical as a solubilizate with Ni^{2+} adsorbed on the micellar surface; the spin exchange in fluid media accompanies the molecular collision between paramagnetic species, which is governed by the diffusional process. To obtain the rate constant of spin exchange and/or that of molecular collision, broadening of the electron spin resonance (ESR) line width of the radical caused by the spin exchange is analyzed with spectra simulation using modified Bloch equations under a consideration of the distribution in Ni^{2+} population per micelle. In the estimation of the lateral diffusion constant from the obtained rate constant, the Ni^{2+} diffusion is modeled as a hopping process on a spherical surface with a finite area. The effect of an environmental exchange of Ni^{2+} between the micellar surface and a bulk aqueous phase on the molecular collision is thoroughly examined by a computer simulation on the model with a Monte Carlo method. The lateral diffusion constant of Ni^{2+} is evaluated to be on the order of 10^{-8} cm^2/s, which is 3 orders of magnitude less than the diffusion constant of Ni^{2+} in ordinary aqueous solutions.

Introduction

It is well-known that ionic surfactant micelles have highly charged surfaces which can adsorb various ionic species through a Coulombic interaction.[1] This is one of properties belonging to a molecular assembly of micelles, not to a single surfactant molecule.[2] From both a scientific and an engineering point of view, information of the bound ions onto the micellar surface is of great importance; the surface charge density of the micelle is a parameter closely related with the formation and stability of ionic micellar assemblies,[3] and the ion binding plays a significant role in the flotation of metal ions.[4] In addition to static parameters, such as the binding degree of ions and the surface charge density, it is crucial to know dynamical ones, such as the mobility of bound ions and surfactant ions in micelles, especially in connection with a nonequilibrium thermodynamical viewpoint of surfactant diffusion.[5] The present study aims at obtaining some dynamical information of the bound ions through an analysis of a spin exchange reaction on the micellar surface.

Spin exchange[6] is one of electron spin-spin interactions, accompanying molecular collision between paramagnetic species in fluid media. From measurement of electron spin resonance (ESR) line widths affected by the spin exchange interaction, the molecular collisional rate constant can be obtained. Moreover, from an analysis of the obtained rate constant on the basis of an appropriate diffusion model, diffusion constants of the paramagnetic species are estimated; this method is advantageous for its applicability to microscopically inhomogeneous media, such as bilayers, microemulsions, and micelles.[7]

In this paper, through an analysis of spin exchange between a hydrophobic nitroxide radical solubilized in a sodium dodecyl sulfate (SDS) micelle and Ni^{2+} adsorbed onto the micellar surface, we will determine the molecular collisional rate constant by ESR spectral simulation with modified Bloch equations.[8] In addition, we will estimate the Ni^{2+} diffusion constant on the micellar surface

---

[1] Tomlinson, E.; Davis, S. S.; Mukhayer, G. I. In *Solution Chemistry of Surfactants*; Mittal, K. L., Ed.; Plenum: New York, 1979; Vol. 1, pp 3-45.

[2] Gustavsson, H.; Lindman, B. *J. Am. Chem. Soc.* **1975**, *97*, 3923.

[3] Shinoda, K.; Nakagawa, T.; Tamamushi, B.; Isemura, T. *Colloidal Surfactant*; Academic Press: New York, 1963; Chapter 1.

[4] Sebba, F. *Ion Flotation*; Elsevier: Amsterdam, 1962.

[5] Mikati, N. *Chem. Phys. Lett.* **1986**, *123*, 51.

[6] Molin, Yu. N.; Salikhov, K. M.; Zamaraev, K. I. *Spin Exchange*; Springer-Verlag: Berlin, 1980.

[7] Keith, A. D.; Snipes, W.; Mehlhorn, R. J.; Gunter, T. *Biophys. J.* **1977**, *19*, 205.

[8] Sachse, J.-H.; Marsh, D. *J. Magn. Reson.* **1986**, *68*, 540.

0022-3654/92/2096-3902$03.00/0